Direct Writing By Way of Melt Electrospinning

Toby D. Brown, Paul D. Dalton, and Dietmar W. Hutmacher**

A decade has passed since solution electrospinning, which has increasingly diverse utility,[1] was proposed as a method to design and fabricate scaffolds for tissue engineering (TE) applications.[2] In most cases, non-woven meshes of sub-micrometer diameter fibers, which resemble the fibrils found in native extracellular matrix (ECM), are collected.[3] However, the low pore sizes associated with the random layering of sub-micrometer diameter fibers is a fundamental issue for solution electrospun meshes, which act as a barrier to cell infiltration rather than promoting it. An important study by Mikos and colleagues demonstrated that, assuming randomly deposited fibers, fiber diameters must be at least 4 μm to design and fabricate a scaffold with a pore size of at least 20 μm in order to promote cell invasion and growth.[4] This limiting factor can be attributed to the nature of the solution electrospinning process. As the polymer solution is electrostatically drawn into a jet, following an initially straight stable zone, bending instabilities develop in a secondary zone along the flight path of the charged jet.[5] Although this results in ultrafine fibers, it causes a relatively large area of collection characterized by chaotic deposition. As a consequence, solution electrospun meshes are usually thin and their assembly is random.[6] There are, however, approaches for the organized deposition of solution electrospun fibers reported in the literature.[7–11] While each of these methods provides reasonably ordered structures, charge accumulation effects on solution electrospun fibers tend to restrict the amount of layers which can be collected and remain bound as one coherent structure.[12]

One method to improve the control over the location of electrospun fiber deposition is to operate in the region of the jet where the flight path is straight. For polymer solutions this requires reducing the distance to the collector to below that at which bending instabilities develop,[13–18] however, this limits the ability to remove solvent from the process by evaporation. Alternatively, polymer melts, typically with higher viscosities and lower conductivities compared to polymer solutions, can be electrostatically drawn over relatively large distances while maintaining a straight jet path.[19] Greater disturbance forces are required to overcome the surface tension in these jets, resulting in extended regions of stability up to many centimeters in length.[20–21] Ultimately the melt electrospun fiber tends to be larger than the solution electrospun one, although there are exceptions to this rule.[19] As shown by Mikos et al., however, an increase in fiber diameter facilitates increased pore size and interconnectivity, which has benefits for scaffold design.[4]

In the research described here, the predictable deposition location of several types of melt electrospun fibers is combined with an automated laterally translating collection system to create a direct writing process which allows the design and fabrication of scaffolds with controllable architectures and patterns. Over a range of fiber diameters, from single micrometer magnitudes to 50 μm, we demonstrate that as the melt electrospinning jet deposits it can be drawn into continuous straight lines, with optimal control when the collector translates at speeds matching the jet speed. Furthermore, these lines can consistently be laid on top of each other to reproducibly build three-dimensional (3D) lattices for biomedical applications, with dimensions that allow cell and tissue invasiveness.

Through manipulation of the melt electrospinning process parameters such as spinneret diameter, voltage, and collector distance, the diameter of the resultant fiber can be controlled for different materials (Table S1, Supporting Information).[22] One of the prime considerations is the combination of melt temperature (which influences the melt viscosity) and extrusion rate, which together determine the filament stability and are reported to have the most significant influence on fiber diameter.[22] For example, as described by Charuchinda et al., poly(ε-caprolactone) (PCL) has a wide melt processing range owing to its low melting point (60 °C) and high thermal stability.[23] In such a case, it is preferable to choose a spinning temperature near the lower end of the range, because the higher the temperature, the more heat that needs to be removed from the electrospun fiber as it cools.

Starting with the case where the melt temperature is fixed at 70 °C. At a mass flow rate of 50 μL h^{-1}, melt electrospinning of PCL (CAPA 6500C, M_w = 50 kDa, Perstorp Ltd, UK) onto a stationary collector results in smooth uniform fibers with an average diameter of approximately 21 μm (where the spinneret inner diameter, voltage, and collector distance are fixed at 0.514 mm (21 G needle), 12 kV, and 30 mm respectively). **Figure 1**a shows lines of such fibers when they are deposited onto a flat collector which translates below a stationary spinneret. A constant translation speed (horizontal direction in Figure 1a) is assigned to each fibrous line, with the speed increased between lines from top to bottom with the following values: 0.01, 0.05, 0.1, 0.2, 0.5, and 1 m min^{-1}, respectively. Typically, when the melt jet deposits onto a stationary surface, it exhibits a straight profile with a buckling region close to the collector caused by axial compression as the jet impacts the collector. Buckling causes the jet to deposit as randomly oriented coils, so that the point of contact between the jet and the collector varies away from that point directly beneath the electrospinning spinneret.[13] When the collector is moved laterally in a straight path, the jet is observed to behave in a similar manner

T. D. Brown, Dr. P. D. Dalton, Prof. D. W. Hutmacher
Institute for Health and Biomedical Innovation
Queensland University of Technology
60 Musk Avenue, Kelvin Grove, QLD 4059, Australia
E-mail: daltonp@qut.edu.au; dietmar.hutmacher@qut.edu.au

DOI: 10.1002/adma.201103482

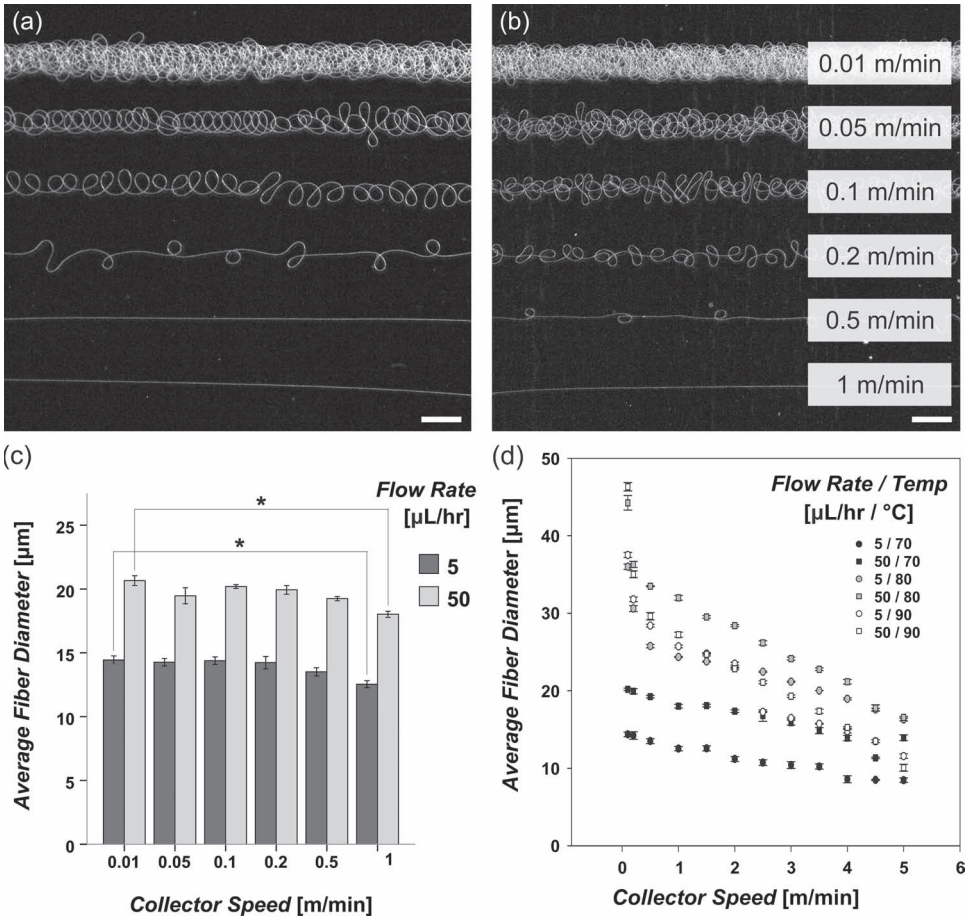

Figure 1. Photograph of lines of PCL fibers melt electrospun at a) 50 and b) 5 µL h^{-1} both at 70 °C. The combination of 12 kV electric field potential and 30 mm collector distance was optimized to maintain the shortest working distance to enable the jet to remain focused without arcing between the collector and spinneret, while allowing adequate distance for the fiber to cool sufficiently and thus solidify. The collector is moving at constant horizontal speeds, increased from top to bottom as indicated for both figures. c) The effect of translation speed on fiber diameter for both flow rates. The experimental data represent the average of five samples with the error bars representing the standard error of the means. Significant differences were found between the fiber diameters at several collector speeds for both flow rates ($p < 0.05$), however, for clarity these differences are indicated only for the highest and lowest speeds on the graph. d) Comparison of fiber diameter for the cases in A) and B) at 70, 80, and 90 °C, where the translation speed is further increased. The experimental data represent the average of five samples with the error bars representing the standard error of the means. Significant differences were found between the fiber diameters between each combination of temperature and flow rate for several collector speeds ($p < 0.05$). A significant difference was also found between the slope of the curves at 90 °C and the remaining curves ($p < 0.05$), However, for clarity these differences are not shown. All scale bars are 1 mm.

to that described for viscous threads falling onto a moving surface.[24–25] As seen in Figure 1a, with increasing translation speed the coiling effects as a result of buckling diminish until the collector speed matches the jet speed at impact (in this case 0.5 m min^{-1}), and the result is a continuous fiber drawn into a straight line with a reduced average diameter of approximately 19 µm.

In Figure 1b, the flow rate is reduced by a degree of magnitude from 50 to 5 µL h^{-1} (the minimum delivery rate achievable in these experiments) and the collector speeds for each line correspond to those in Figure 1a. There is less viscoelastic mass resisting being accelerated towards the collector, causing an increase in jet speed and reduction in fiber diameter. This is accompanied by higher frequency buckling with a reduced coil size.[17] The result is that a faster collector speed of 1 m min^{-1} is required to draw the jet into a straight line. Figure 1c shows average fiber diameters measured for each line in Figure 1a and b, with an approximate one-third reduction in fiber diameter when the flow rate is reduced from 50 to 5 µL h^{-1}. Furthermore, these results indicate that when the flow rate is held constant, increasing the collector speed causes a reduction in fiber diameter because of the introduction of a drawing effect. Figure 1d compares the two previously described cases where the melt temperature is increased from 70 to 80 and 90 °C, respectively, with the collection speed further increased up to 5 m min^{-1}. The viscosity of CAPA 6500C PCL is reported to reduce from 2890 Pa s (10 s^{-1}) at 70 °C to 1353 Pa s (10 s^{-1}) at 100 °C,[26] thus improving the melt flow behavior of the extruded polymer. According to Domingos et al., at temperatures above 90 °C, the flow properties of PCL remain roughly stable.[27] At higher

spinning temperatures over 90 °C, as the melt viscosity further decreases, the fibers do not solidify sufficiently over the 30 mm collector distance prior to deposition and as a result begin to spread non-uniformly on the collector (Figure S1, Supporting Information). When collection speeds are increased, this leads to premature breaking of the electrospinning jet, or fracture of the fiber as it is stretched between fibers across the collection surface (Figure S1, Supporting Information).

In Figure 1d the stationary (or starting) average fiber diameters are greater at a flow rate of 50 μL h^{-1} than at 5 μL h^{-1} for each temperature. However, for a particular flow rate an increase in temperature is causing an increase in initial fiber diameter. This can be explained by the fact that in these experiments a syringe pump, which uses a constant displacement screw to generate flow, was used as the driving mechanism to extrude the polymer melt through a needle. As the temperature increases, the viscosity decreases which means that the polymer flows more readily (provides less resistance to extrusion) through the spinneret for the same syringe pump flow rate setting. Thus, in this case the increasing temperature is having the effect of increasing the fiber diameter through an increased mass delivery rate. Although typically in the literature the syringe pump flow rate is quoted as the experimental flow rate,[21] our results show that further investigation is required to establish a means to characterize the actual mass delivery rate to the electrospinning Taylor cone based on the combination of temperature and device flow rate.

Although an increase in temperature leads to a larger starting fiber diameter, the associated reduction in viscosity causes an increase in elasticity of the jet. Therefore, when the translation speed is increased, there is a greater relative reduction in fiber diameter because the jet is more readily elongated. This is shown in Figure 1d where the initial slopes of the curves are steeper with increasing temperature. In each case, the curves level out with increasing speed and appear to be converging on an ultimate diameter as the fiber is further drawn. However, as will be further discussed, what is of more interest for the development of a melt electrospinning writing process is matching the jet speed with the collector translation speed.

The translation speeds where the collected fibers become straight lines in each case in Figure 1d are: 1, 0.5, 0.36, 0.35, 0.3, and 0.325 (m min^{-1}) for the respective 5/70, 50/70, 5/80, 5/90, 50/90, and 50/80 (μL h^{-1}, °C) flow rate/temperature combinations. For the combination of fixed process parameters described above, the minimum achievable average fiber diameter at the point where the collected fiber becomes straight is 12.5 μm, using a flow rate/temperature combination of 5/70 (μL h^{-1}, °C).

As the collector speed increases towards and beyond the jet speed, the jet profile may be described by a viscous thread "vertical fall" solution.[28] This can be explained by consideration of the forces at work on the jet which determine its profile, and are influenced by the relationship between jet speed (S_J) and collector speed (S_C). **Figure 2**a illustrates schematically the change in shape of the jet profile corresponding to four different relative collector speeds: 1) when the collector is stationary (S_C = 0), the jet's path is straight with a "compressive heel" close to the collector where buckling occurs. This causes the location of deposition to diverge away from the point directly below the spinneret as coiling takes place;[28] 2) the net effect of the compressive force reduces as the collector speed is increased. Drag between the jet and the collector surface introduces an axial tensile force into the jet. When the collector speed is equal to the jet speed ($S_C = S_J$), the heel region in the jet profile has decreased to a balance between the tensile and compressive forces. As a result, the point of deposition moves directly under the spinneret;[28] 3) when the collector speed is increased above the jet speed ($S_C > S_J$), the point of contact between the jet and the collector begins to "lag" behind the point directly below the

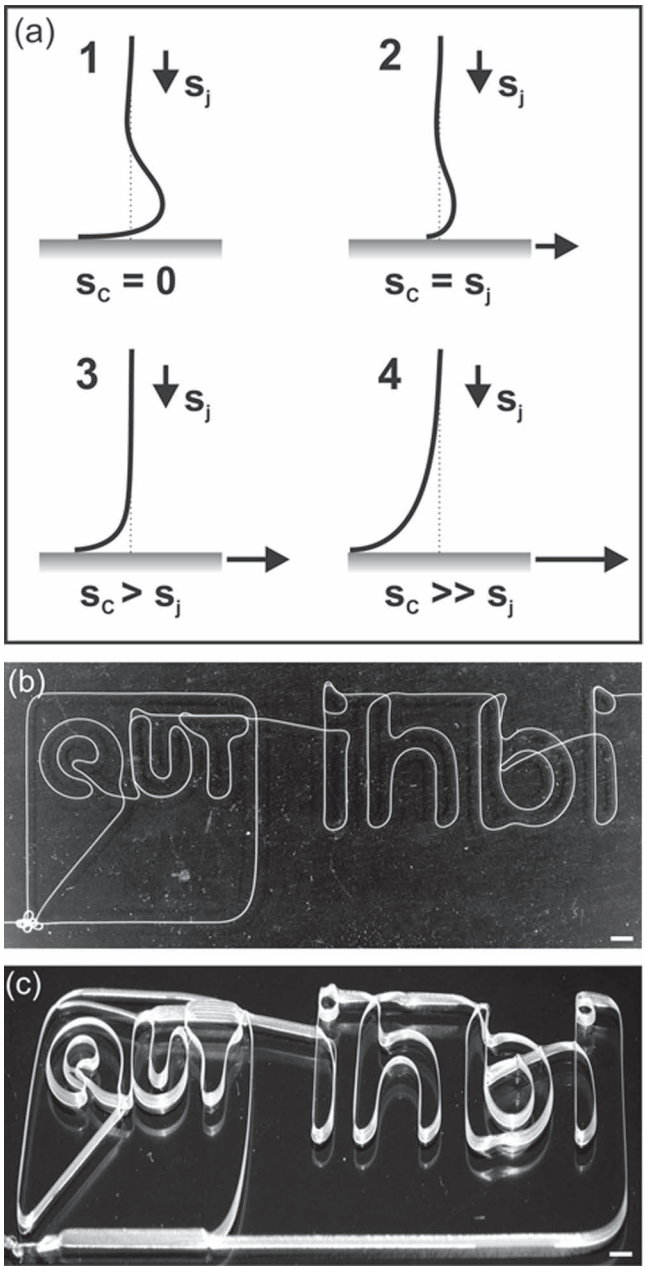

Figure 2. a) Schematic showing that the shape of the melt electrospinning jet profile is dependent on the speed of the collector (S_C) relative to the jet speed (S_J). b) Direct writing of QUT IHBI logo using melt electrospinning. c) Ten layer 3D version of QUT logo. All scale bars 1 mm.

spinneret. Drag dominates the compressive stresses and causes a delayed response as the viscoelastic jet is stretched because of a net axial tensile force.[28] The jet acquires a concave profile, which can be described by a "catenary" solution;[29] and 4) as the collector speed is further increased relative to the jet speed ($S_C >> S_J$), the catenary profile of the jet becomes more pronounced as the distance between the point of deposition and that directly below the spinneret increases, causing further stretching of the jet. This is accompanied by increased error because of the lag effect, if it is assumed that the optimal location of contact between the jet and the collector is directly below the spinneret for the development of a writing process. These results suggest that for a desired combination of melt electrospinning parameters, which may result in different fiber diameters, complex geometries and patterns can be "written" by matching the speed of the translating collector as close as possible to the jet speed.

Figure 2b shows smooth direct writing over an area of 40 mm × 15 mm where the diameter of the fiber is approximately 20 μm. The smoothness of the pattern was achieved by setting the translational speed of the stage as close as possible to the deposition rate (0.5 m min^{-1} as determined from Figure 1c), compensating for acceleration and deceleration at turning points. The controllability and continuity of this process is demonstrated in Figure 2c, which shows the controlled layer-by-layer deposition of fibers: where the same pattern is repeatedly laid down on top of itself ten times to create a 3D construct.

One strategy adapted from additive manufacturing (AM) methods (reviewed in detail by Woodruff and Hutmacher),[30] involves the definition of a "unit pattern" which can be written in successive additive layers to build up a 3D structure, suitable as a TE scaffold. An example is to write a series of parallel lines in one direction, then for the next layer, orient these lines perpendicular to the layer before using a "woodpiling" technique.[31] However, considering the process involves writing with a continuous filament, one method to achieve parallel lines is to write a square wave pattern. Illustrated schematically in **Figure 3**a(1), each step in the square wave allows the jet to turn in between tracing successive parallel lines back and forth. The ability to change direction in such a manner requires deceleration of the collector towards the turning points, hence a reduced turning speed, and then acceleration up to the straight line collector speed. Figure 3a(2,3) demonstrate the importance of "matching" the step or turning speed (S_T) to the straight line speed (S_C) by showing three attempts to write (horizontal) parallel fibers using the square wave pattern represented in Figure 3a(1).

In this case, the electrospinning conditions from Figure 1d, with flow rate/temperature combination of 5/80 (μL h^{-1}, °C) were used, where the needle inner diameter was reduced to 0.337 mm (23 G). This demonstrates another method to further reduce the mass delivery rate, yielding fibers with an average diameter of 5 μm. Reducing the temperature to 70 °C results in a further decrease in average fiber diameter to between 1 and 2 μm where collector speeds around 5 m min^{-1} are required to write straight lines. The automated stage was programmed to translate over an area of 10 mm × 10 mm at 10 μm steps and a constant horizontal speed where, because of the increase in jet speed associated with reduced fiber diameter, S_C = 3 m min^{-1} yields straight fibers. Only S_T is varied. In Figure 3a(2), for S_T = 0.1 m min^{-1}, although this speed is significantly less than that required to draw the jet into a straight line, insufficient time is provided over the turning distance for the jet to respond to a change in direction before it is dragged back in the opposite horizontal direction. There is a delayed response to variations in the forces experienced by the jet because of its viscoelastic nature, combined with the lag effect described in Figure 2a. The result in Figure 3a(2) is that the jet never reaches the end of each parallel path as prescribed by the translation of the stage. In contrast, as shown in Figure 3a(3), S_T = 0.002 m min^{-1} provides more time for the jet to respond to a change in direction than is required. The additional time allows buckling effects to take place, as seen at both ends of the fibrous pattern where randomly coiled fibers reduce the effective area of the desired pattern. There is also sufficient time for a secondary effect characteristic to electrospinning to prevail: coulombic repulsive forces between fibers result in a (lower frequency relative to the buckling frequency) pendulum motion of the jet and further reduce the useful area of the square wave pattern.[32] This effect is illustrated at the top left corner of the patterns in Figure 3a(2,4), where the writing process is stationary and the area of random fiber deposition grows in a circular manner.[33] Figure 3a(4) demonstrates the results when S_C and S_T are matched. In this case S_T = 0.005 m min^{-1} and the resultant fibrous pattern corresponds to the area prescribed.

The matching S_T will vary as S_C changes. For example, using the same electrospinning conditions from Figure 1d, with the flow rate/temperature combination of 5/70 (μL h^{-1}, °C) for another type of PCL (M_n = 80 000, Sigma–Aldrich, Australia) causes an increase in resultant fiber diameter from 12.5 to 20 μm. The associated increase in molecular weight is accompanied by increased viscosity,[34] where the jet provides greater resistance to being drawn by the electrostatic field and subsequently its speed is reduced. Therefore, the corresponding straight line collector speed S_C = 0.5 m min^{-1} (Figure 1c) is slower, similar to the 50/70 (μL h^{-1}, °C) case in Figure 1d. A reduced turning speed S_T = 0.002 m min^{-1} was determined to match S_C.

The advantage of this slightly larger fiber diameter is that it more readily facilitates the fabrication of a scaffold with relevant thickness. In Figure 3b, fifty continuous layers of such parallel fibers were written in one orientation and then the pattern was rotated 90° and another fifty layers written. The straight line length of the pattern was increased to 30 mm so that the turning regions at each end of the pattern would not interfere with the area where the fibrous layers cross. This process allows the fabrication of a periodic lattice, with dimensions 10 mm × 10 mm in the central square, with a thickness of approximately 1 mm.

Figure 3c demonstrates a similar amount of fibrous layers as in Figure 3b stacked directly on top of each other with precise control to create an ordered architecture approximately 1 mm thick, where electrostatic effects cause a loss of control over fiber deposition. Figure 3d shows a combination of interweaving and fusion between the fibers in Figure 3c which may improve the structural integrity of melt electrospun scaffolds.

One limitation of using a square wave approach is that these curved turning paths may have a minimum diameter for a set of operating parameters, which in turn limits the achievable

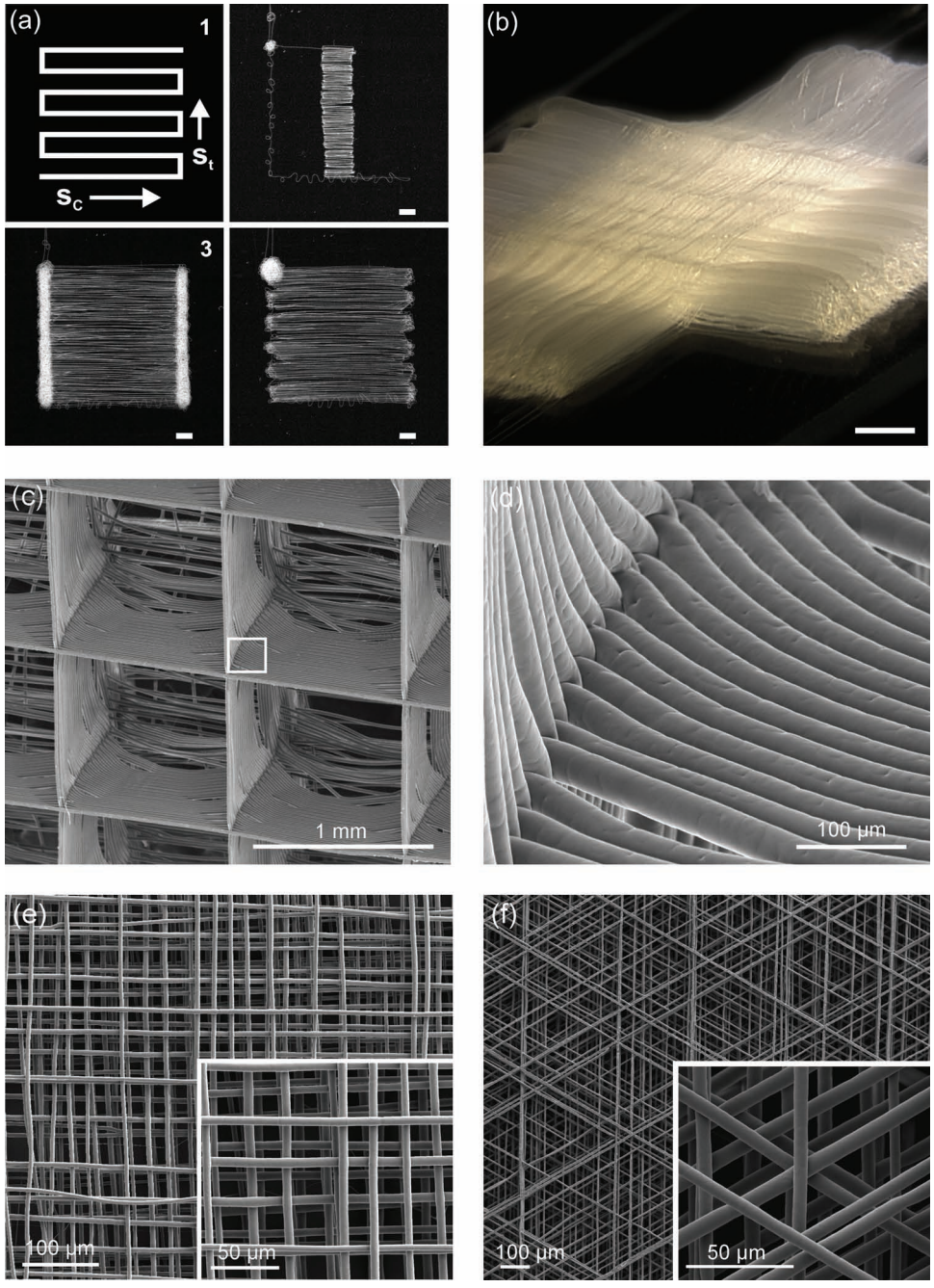

Figure 3. a) Schematic representing the programmed square wave pattern translated by *x*–*y* stage. PCL fibers drawn with constant straight line speed (S_C) and turning speed (S_T) varied at 2) 0.1, 3) 0.002, and 4) 0.005 m min^{-1}. Scale bar 1 mm. b) Photograph of a scaffold created using a square wave pattern with alternating series of layers oriented at 90°. Scale bar 1 mm. Scanning electron microscopy (SEM) images of c) the stacking and d) interweaving of fibers to form an array of 1 mm × 1 mm × 1 mm boxes. PCL scaffolds assembled with fibrous layers oriented at E) 90° and F) 60°.

in plane pitch, i.e., the distance between successive straight fibers. This is because of the lag effect described in the previous square wave writing approach, combined with the delayed viscoelastic response associated with turning the path of the electrospinning jet, where the actual turning regions are curved rather than square as translated by the collector (Figure S2, Supporting Information). In order to overcome this effect, the fiber diameter can be reduced. Returning to the settings used in Figure 3a, 5 µm diameter fibers can be written in parallel with a minimum turning diameter of 60 µm. By writing successive layers oriented at 90° and introducing a 20 µm offset per layer (so that the same path is traced by the stage after every sixth iteration), a lattice architecture represented in Figure 3e can be fabricated with control over fiber placement up to 300 µm in thickness. The result is a periodic structure with an apparent pore size of 20 µm. This strategy also helps to improve the

interconnectivity of pores (rather than creating the "walls" of stacked fibers shown in Figure 3d which would provide a barrier to cell invasion), as there are five other fibers building up the thickness before the next fiber is written along the same path by the stage. To further improve pore interconnectivity, more layers at different orientations can be introduced into the lattice design. For example, in Figure 3f a similar process is followed to that described in Figure 3e, however, successive layers are oriented at 60° so that now eight fibers lie between the repeating fibers.

Melt electrospinning is similar to other melt-based AM approaches where a filament is extruded continuously through an orifice. In AM approaches such as fused-deposition modeling (FDM), the final filament diameter is largely determined by the nozzle diameter (Table S2, Supporting Information). For very small nozzle diameters (i.e., <100 μm), the pressures required to achieve a suitable flow rate can be beyond those practically possible.[35] The addition of high voltage to this process characteristic to melt electrospinning enables the emerging filament to be drawn electrostatically, reducing the deposited fiber diameter by two orders of magnitude, thus offering significant improvements in filament resolution. Whereas in AM techniques such as FDM the achievable filament resolution is above 100 μm, requiring collection speeds generally less than 1 m min^{-1}, in this work we have demonstrated that fibers with single micrometer resolution can be accurately located using collection speeds five times faster.

In conclusion, we were able to accurately deposit melt electrospun PCL fibers to create complex porous structures using an automated stage. Matching the translation speed of the collector to the speed of the melt electrospinning jet is the key factor which establishes control over the location of fiber deposition in order to write with a continuous line. We have demonstrated for the first time that melt electrospun fibers can consistently be laid on top of each other to create scaffolds in a manner comparable to many of the melt-extrusion based direct writing processes used in AM and, therefore, this direct writing method can be considered an addition to AM. However, in this case the filament resolution and fiber to fiber distances achievable are approaching sub-micrometer magnitudes. In this sense, melt electrospinning writing can be seen to bridge the gap between solution electrospinning and direct writing AM manufacturing processes.

Experimental Section

Materials: PCL (M_n = 80 000) (Batch #12331AB) and PCL (M_w = 50 kDa) (Lot #41029) were purchased from Sigma–Aldrich (Australia) and Perstorp, UK Ltd (United Kingdom), respectively, and used as received without any further treatment.

Electrospinning: PCL pellets were loaded into a plastic Luer-lock 3 mL syringe (B-Braun, Australia). The syringe was placed in a custom Plexiglass water jacket housing (Labglass, Australia) through which heated water (70 to 90°C) was circulated using a recirculating water tank (Ratek, Australia). The syringe was heated for one hour to provide a homogeneous polymer melt. Hypodermic needles (21 and 23 G) (Becton Dickinson, Australia) were attached to the syringe to be used as the spinneret. The feeding rate of the polymer melt in the syringe (5 to 50 μL h^{-1}) was controlled using a programmable syringe pump (World Precision Instruments, USA). Voltages up to 12 kV were applied to the needle. The distance between the tip of the needle and the collector was 30 mm. A 2 mm thick, 12 mm × 12 mm aluminum plate was used as a grounded collector, mounted onto two linear slide assemblies (Velmex Inc., USA) in an *x*–*y* configuration. Custom translation patterns were written in G-code and controlled using Mach3 motion control software (Artsoft, USA). Translation velocities ranged up to 5 m min^{-1}.

Morphology Observation: Scaffold surfaces were sputter coated with gold (10 nm thick) using a Leica Microsystems EM SCD005 (Germany) and scanning electron microscopy (SEM) examination carried out using an FEI Quanta 200 Environmental SEM (Netherlands) at an accelerating voltage of 10 kV. Optical images were taken using a Canon EOS 450D digital single lens reflex (DSLR) camera with a Canon EF-S 60 mm f/2.8 Macro USM lens (Canon.Inc, Australia). Images were prepared and processed using Corel DRAW and PHOTO-PAINT X4 (Corel Corporation, Australia) and Adobe Photoshop and Illustrator CS4 (Adobe Systems Incorporated, Australia) using image auto-adjust functions. The images in Figure 1a and b were imported into Image J software (NIH, USA) and the fiber diameter for each line measured at five random locations. Mean fiber diameters, standard error of the means, and differences between the means (using one-way ANOVA with the assumption of normally distributed data) were then calculated using PASW Statistics 18 software (SPSS Inc., USA).

Supporting Information

Supporting Information is available from the Wiley Online Library or from the author.

Acknowledgements

The authors are grateful for the assistance of Dr Christina Theodoropoulos (SEM imaging) and Anna Slotosh for generating the pattern for the QUT IHBI logo. The AO Foundation provided funding to support this research (RM: 2010002533).

Received: September 9, 2011
Published online: November 18, 2011

[1] S. Agarwal, J. H. Wendorff, A. Greiner, *Adv. Mater.* **2009**, *21*, 3343.
[2] W. J. Li, C. T. Laurencin, E. J. Caterson, R. S. Tuan, F. K. Ko, *J. Biomed. Mater. Res. A* **2002**, *60*, 613.
[3] A. Cipitria, A. Skelton, T. R. Dargaville, P. D. Dalton, D. W. Hutmacher, *J. Mater. Chem.* **2011**, *21*, 9419.
[4] Q. P. Pham, U. Sharma, A. G. Mikos, *Biomacromolecules* **2006**, *7*, 2796.
[5] Y. M. Shin, M. M. Hohman, M. P. Brenner, G. C. Rutledge, *Appl. Phys. Lett.* **2001**, *78*, 1149.
[6] D. H. Reneker, A. L. Yarin, H. Fong, S. Koombhongse, *J. Appl. Phys.* **2000**, *87*, 4531.
[7] P. D. Dalton, D. Klee, M. Moller, *Polymer* **2005**, *46*, 611.
[8] D. Zhang, J. Chang, *Adv. Mater.* **2007**, *19*, 3664.
[9] C. Vaquette, J. J. Cooper-White, *Acta Biomater.* **2011**, *7*, 2544.
[10] W. E. Teo, M. Kotaki, X. M. Mo, S. Ramakrishna, *Nanotechnology* **2005**, *16*, 918.
[11] N. J. Amoroso, A. D'Amore, Y. Hong, W. R. Wagner, M. S. Sacks, *Adv. Mater.* **2011**, *23*, 106.
[12] S. Ramakrishna, K. Fujihara, W. E. Teo, T. C. Lim, Z. Ma, *An Introduction to Electrospinning and Nanofibers*, World Scientific Publishing, Singapore **2005**.
[13] T. Han, D. H. Reneker, A. L. Yarin, *Polymer* **2007**, *48*, 6064.
[14] J. Kameoka, R. Orth, Y. Yang, D. Czaplewski, R. Mathers, G. W. Coates, H. G. Craighead, *Nanotechnology* **2003**, *14*, 1124.

[15] D. H. Sun, C. Chang, S. Li, L. W. Lin, *Nano Lett.* **2006**, *6*, 839.
[16] C. Chang, K. Limkrailassiri, L. W. Lin, *Appl. Phys. Lett.* **2008**, 93.
[17] G. F. Zheng, W. W. Li, X. A. Wang, D. Z. Wu, D. H. Sun, L. W. Lin, *J. Phys. D: Appl. Phys.* **2010**, 43.
[18] C. Hellmann, J. Belardi, R. Dersch, A. Greiner, J. H. Wendorff, S. Bahnmueller, *Polymer* **2009**, *50*, 1197.
[19] H. Zhou, T. B. Green, Y. L. Joo, *Polymer* **2006**, *47*, 7497.
[20] P. D. Dalton, D. Grafahrend, K. Klinkhammer, D. Klee, M. Moller, *Polymer* **2007**, *48*, 6823.
[21] D. W. Hutmacher, P. D. Dalton, *Chem. Asian J.* **2011**, *6*, 44.
[22] N. Detta, T. D. Brown, F. K. Edin, K. Albrecht, F. Chiellini, E. Chiellini, P. D. Dalton, D. W. Hutmacher, *Polym. Int.* **2010**, *59*, 1558.
[23] A. Charuchinda, R. Molloy, J. Siripitayananon, N. Molloy, M. Sriyai, *Polym. Int.* **2003**, *52*, 1175.
[24] S. W. Morris, J. H. P. Dawes, N. M. Ribe, J. R. Lister, *Phys. Rev. E: Stat. Nonlinear Soft. Matter. Phys.* **2008**, *77*, 066218.
[25] N. M. Ribe, J. R. Lister, S. Chiu-Webster, *Phys. Fluids* **2006**, *18*, 124105.
[26] E. Rudnik, *Compostable Polymer Materials*, Elsevier Science, Oxford, **2008**.
[27] M. Domingos, F. Chiellini, A. Gloria, L. Ambrosio, P. Bartolo, E. Chiellini, *Innovative Developments in Design and Manufacturing: Advanced Research in Virtual and Rapid Prototyping*, Taylor & Francis, Oxford **2009**, pp. 67–73.
[28] M. J. Blount, J. R. Lister, *J. Fluid Mech.* **2011**, *674*, 489.
[29] M. Bergou, B. Audoly, E. Vouga, M. Wardetzky, E. Grinspun, *ACM Trans. Graph.* **2010**, *29*, 116.
[30] M. A. Woodruff, D. W. Hutmacher, *Prog. Polym. Sci.* **2010**, *35*, 1217.
[31] J. A. Lewis, *Adv. Funct. Mater.* **2006**, *16*, 2193.
[32] T. Han, D. H. Reneker, A. L. Yarin, *Polymer* **2008**, *49*, 2160.
[33] P. Heikkila, L. Soderlund, J. Uusimaki, L. Kettunen, A. Harlin, *Polym. Eng. Sci.* **2007**, *47*, 2065.
[34] M. P. Grosvenor, J. N. Staniforth, *Int. J. Pharm.* **1996**, *135*, 103.
[35] T. B. F. Woodfield, J. Malda, J. De Wijn, F. Peters, J. Riesle, C. A. Van Blitterswijk, *Biomaterials* **2004**, *25*, 4149.